Kovove Mater. 60 2022 303–314
DOI: 10.31577/km.2022.5.303

Effect of tempering process on mechanical properties of high titanium microalloyed steels containing niobium

Xiaopei Guo[1,2], Tao Li[3]*, Zhiqiang Shang[1,2], Guannan Li[1,4], Yafeng Li[5]

[1] *College of Materials Science and Engineering, Chongqing University, Chongqing 400044, P. R. China*
[2] *Chongqing Key Laboratory of Vanadium-Titanium Metallurgy and Advanced Materials, Chongqing University, Chongqing 400044, P. R. China*
[3] *College of Metallurgy and Energy, North China University of Science and Technology, Tangshan 063000, P. R. China*
[4] *Technical center, Handan Branch of Hegang Company Limited, Handan 056015 P. R. China*
[5] *Xinzhou Comprehensive Inspection and Testing Center, Xinzhou, Shanxi, 034000 P. R. China*

Received 7 June 2022, received in revised form 13 July 2022, accepted 5 September 2022

Abstract

This paper focuses on the thermodynamic behavior of the precipitation of the second phase and microstructure evolution of the high titanium microalloyed steel containing niobium during tempering in the temperature range of 500–650 °C to reveal the influence of the heat treatment scheme on the toughness and microhardness. The results indicate that FCC_A1#2 phase is isomorphic to FCC_A1#3, which are carbonitrides of Ti or Nb, and precipitates at about 1266 °C. The Ti and Nb elements almost entirely precipitated at 800 °C, and their contents in the FCC_A1#2 phase are much higher than those in FCC_A1#3 in the low-temperature region. The microstructure of the tempered samples is mainly composed of granular bainite (GB), on which martensite/austenite (M/A) islands are distributed. The decomposition extent of M/A islands got higher and transformed into a large number of nano-sized cementite distributed at the grain boundaries of ferrite with the increasing tempering temperature. It is noticeable that those nanoscale spherical carbide particles provide an effective way to enhance the low temperature impact toughness of the steel significantly. The nanoparticles in the experimental steel tempered at 600 °C have an average diameter of 4.4 nm, accounting for nearly 65 % of the total number of particles. The experimental steel manifested the best low-temperature impact toughness of 361 J with a tempering temperature of 600 °C for 60 min after being quenched from 900 °C.

K e y w o r d s: thermodynamics, precipitation, microstructure, property, heat treatment

1. Introduction

Steel is one of the world's most crucial and popular materials due to its excellent mechanical properties, process properties, and economic practicality, which significantly contribute to the development of industries and the progress of society [1, 2]. It is imperative to develop high-quality steel with advanced comprehensive mechanical properties and low cost [3, 4]. In recent years, metallurgical scientists have developed high-strength microalloyed steel with low carbon (C) content based on the recognition that the high strength and toughness of steel can be realized with low alloy consumption [4]. The high-strength microalloyed steel is widely used in many fields and is mainly alloyed with titanium (Ti), niobium (Nb), and vanadium (V) individually or associated [5].

Niobium is the most effective element for improving the properties of microalloyed steel, which generally exists in the form of solute atoms or precipitated phases [6–8]. The migration rate of the crystal boundaries could be significantly reduced by the solute drag effect of Nb, which would slow down the grain growth rate. In addition, Nb could precipitate with C or N to form nano precipitates, such as niobium carbide (NbC) and niobium nitride (NbN), which could nail the grain boundary of austenite and delay the recrystallization process of austenite, to achieve the pur-

*Corresponding author: e-mail address: litao0518@hotmail.com

Table 1. The chemical component of Nb-Ti composite microalloyed steels (wt.%)

Elements	C	Si	Mn	P	S	Nb	Ti	Als	Ca	N
Content	0.075	≤ 0.10	≤ 1.25	≤ 0.012	≤ 0.002	0.025	0.10	0.025	0.003	< 0.005

pose of refining the microstructure after phase transformation during thermal processing of steel [9]. Due to the high price of Nb and V, an increasing number of researchers have focused on the study of microalloyed steels with Ti as the primary alloying element recently, especially on the precipitation behavior of the second phase, thermo-mechanical control process (TMCP), microstructure and properties of Ti microalloyed steels [10–12]. Generally, Ti is added in combination with Nb for their coupling effect of grain refining and precipitation hardening. Hu et al. [13] studied the influence of the cooling mode on the precipitation of the second phase and properties of the Ti-Nb microalloyed steel, which included the former-fast-cooling (FFC) and later-fast-cooling (LFC) mode. The results indicated that the microstructure of LFC samples consisted of smaller bainite plates and more uniformly distributed small martensite/austenite (M/A) islands compared with that of the FFC samples. In addition, the precipitates in the LFC samples were more and smaller than those in the FFC samples, which finally achieved better mechanical properties. Gan et al. [9] quantitatively analyzed the effects of Ti content on microstructure and the strength of Nb-Ti microalloyed steel, which revealed that the strength was significantly improved with the increase of Ti from 0.041 to 0.079 % due to the strengthening effects of grain refinement, precipitation, and dislocation.

It is well recognized that the composition, size, distribution, and volume fraction of the second phase particles controlled by the thermodynamic equilibrium contribute largely to controlling and improving the microstructure and mechanical properties of the steel products [13–17]. The thermodynamic and kinetic analysis of the solid solution and precipitation behavior of the microalloying elements in steel, as well as modeling and simulation, have been studied by researchers for many years [18–20]. Han et al. [7] investigated the precipitation behavior of Ti in low C medium manganese steel treated by various processes and discovered that the dislocation strengthening mechanism induced by TiC precipitation is dominant for the variation of both strength and toughness. Wang et al. [20] investigated the thermodynamic behavior of the solid solution and coupling precipitation of the microalloying elements in 50CrVA spring steel at different temperatures and built the quantitative relationship between the contents of various microelements and the secondary phase as well as their effect on fatigue life. Luo et al. [18] established a thermodynamic model to predict the austenite/carbonitride equilibrium in the Fe-Nb-C-N alloy system, which mainly calculated the equilibrium volume fraction and chemical driving force of carbonitrides of each element in austenite. However, there are few reports for the high Ti microalloyed steels containing Nb on the microstructure evolution during heat treatment, as well as the effect on the mechanical properties. Therefore, it is necessary to comprehensively investigate the relationship between the precipitation behavior of the second phase particles and the mechanical properties of the high Ti microalloyed steels containing Nb during the tempering process.

In the current work, the precipitation behavior of the second phase particles is investigated systematically in the hot-rolled Nb-Ti microalloyed steel along the balanced cooling process by using Thermo-Calc software. The low-temperature impact toughness and microhardness of the experimental steel were detected by different tempering processes after quenching. Meanwhile, the evolution of microstructure was analyzed based on the observation using optical microscopy (OM) and scanning electron microscopy (SEM). In addition, the fine structure and nano precipitates in the tempered microstructure were characterized by transmission electric microscopy (TEM), and the mechanism of their effect on the mechanical properties was discussed in detail.

2. Experiment

2.1. Materials and process

The chemical composition of Nb-Ti microalloyed steel is presented in Table 1, among which the mass content of Ti is up to 0.1 %. The billets were produced by converter smelting followed by the ladle furnace (LF) refining, vacuum refining, and continuous casting, which were then placed in a furnace at a temperature of 1250 $\pm$ 20 ℃ to soak for a specific time. The microalloying elements were sufficiently dissolved in the austenite. Subsequently, rough rolling, finishing rolling, and coiling processes were performed to obtain the final rolled products. The exact values of the processing parameters of rolling are listed in Table 2.

Several samples with the size of $13 \times 13 \times 65\,\mathrm{mm}^3$ were machined by electro-spark wire-electrode cutting from the steel. The samples were subjected to a furnace that had been heated to 900 ℃ to keep for

Table 2. The processing parameters of rolling

Processing	Soaking	Rough rolling	Medium rolling	Finishing rolling	Crimping
Temperature (℃)	1250 ± 20	1200 ± 15	980 ± 15	860 ± 15	600 ± 15

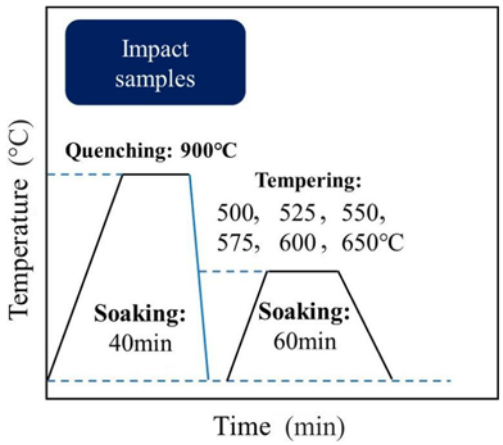

Fig. 1. Heat treatment schematic.

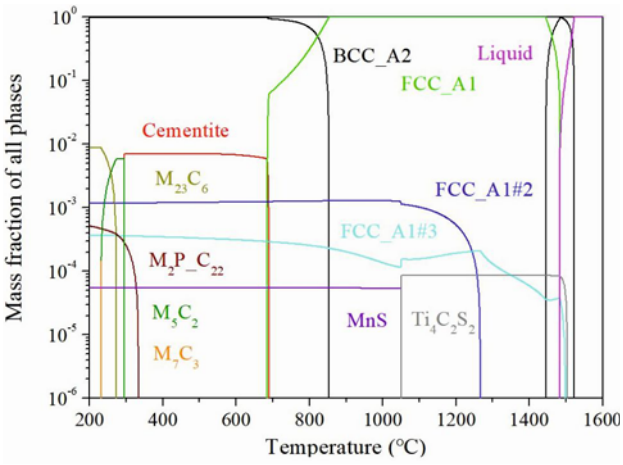

Fig. 2. Relationship between the precipitation of the second phase and temperature.

40 min and then cooled to room temperature by water, which aimed to avoid grain growth. Three samples treated by quenching were taken as a group and were then tempered at different temperatures (500, 525, 550, 575, 600, and 650 ℃ for 60 min, as shown in Fig. 1, to reduce the stress inside the samples and improve the comprehensive mechanical properties. Finally, the samples after the heat treatment above were processed into the standard samples ($10 \times 10 \times 55\,mm^3$) for impact test and small pieces with a size of $10 \times 10 \times 5\,mm^3$ for metallographic observation, respectively.

2.2. Mechanical properties

To evaluate the mechanical properties of the samples after heat treatment, a Charpy V-notch impact test at –20 ℃ was conducted, assisted by liquid nitrogen cooling on a metal pendulum impact tester. Three samples were tested for each heat treatment process to guarantee reproducibility. Meanwhile, the values of the microhardness of the samples were obtained by the Vickers hardness tester, which were taken from an average of eight different locations on the sample surface.

2.3. Microstructure characterization

The samples for metallographic observation were ground with sandpapers and polished by diamond polishing spray. The 4 vol.% nital solution was used to etch the surface of polished samples to reveal microstructure. The microstructure of metallographic samples was characterized by OM and SEM.

A slice of 0.6 mm in thickness was cut from the metallographic sample using a wire-cutting electrodischarge machine for further TEM examination. These samples were punched into discs with a diameter of 3 mm. Then, the thin wafer was manually ground to a thickness of less than 100 μm and further thinned into about 30 μm using a pit lapping machine. Finally, the TEM foils were prepared by an ion thinning instrument. The foils were observed under the FEI Talos F200X TEM with an energy dispersive spectrometer (EDS) attachment operated at 200 keV to investigate the composition, morphology, and distribution of the precipitates in the steel treated by quenching and tempering process.

3. Results and discussion

3.1. Thermodynamic analysis of the second phase particles

The precipitation behavior of the second phase particles in the experimental steel was calculated in the range of 200–1600 ℃, using *Thermo-Calc thermodynamic calculation software*. Figure 2 shows the relationship between the contents of the second phase and the temperature. The logarithmic ordinate more obviously reflects the change of the theoretical contents of

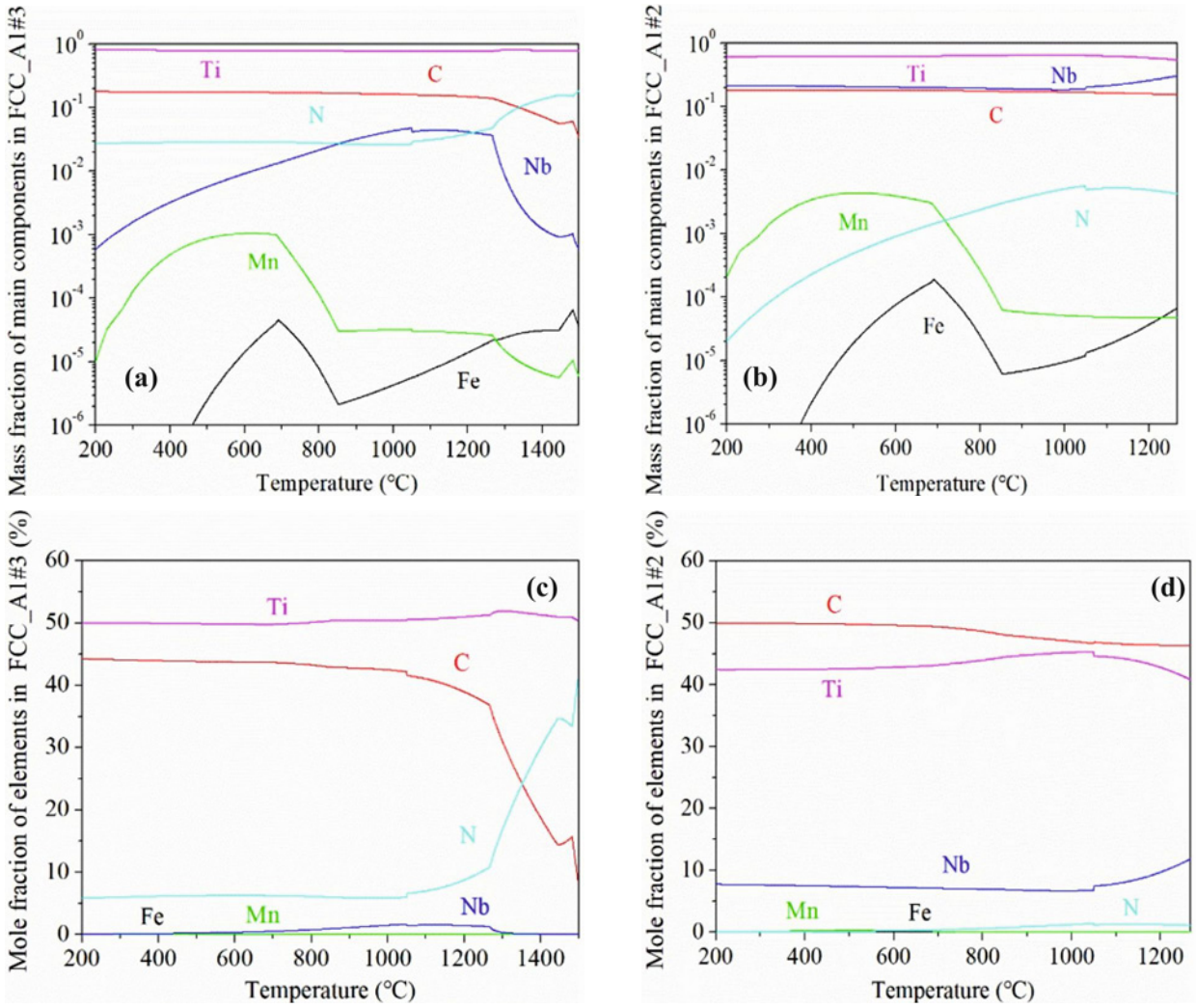

Fig. 3. Relationship between the content of elements in the phases and temperature: (a), (c) FCC_A1#3; (b), (d) FCC_A1#2.

the precipitated second phase. The second phase precipitated with the decreasing temperature during the equilibrium cooling process of the experimental steel, mainly including $Ti_4C_2S_2$, FCC_A1#3, FCC_A1#2, MnS, cementite, $M_2P\_C_{22}$, M_5C_2, $M_{23}C_6$, and M_7C_3. The $Ti_4C_2S_2$, cementite, etc., only exist in a specific temperature range, which are the transitional phases. FCC_A1#3, FCC_A1#2, and MnS phases precipitate continuously over a wide temperature range. The equilibrium precipitation temperatures of $M_2P\_C_{22}$, M_5C_2, $M_{23}C_6$, and M_7C_3 phases are beyond the experimental temperature range, and the precipitation temperatures of MnS and $Ti_4C_2S_2$ are far less than those of FCC_A1#3 and FCC_A1#2, which are focused in the discussion below.

After the FCC_A1#3 phase begins to precipitate during the solidification of the liquid steel, the amount increases rapidly and then decreases in a small range around 1450 ℃, then continues to rise and reaches a small peak near the temperature of 1266 ℃, at which FCC A1#2 phase begins to precipitate. It could be seen from Fig. 3 that the main components of FCC_A1#3 include Ti, C, N, Nb, and trace amounts of Fe and Mn. The content of Nb is two orders of magnitude lower than that of Ti in FCC_A1#3. Moreover, the mole fraction of Ti is almost equal to the sum of the mole fraction of C and N; thus, the stoichiometric ratio of the Ti, C, and N in the FCC_A1#3 could be assumed to be in the form of Ti (C, N). The proportion of Ti in FCC_A1#3 is relatively stable, about 80 %. The proportion of N is larger than that of C at the beginning of the precipitation stage, indicating that it is mainly in the form of TiN at high temperatures, and more N atoms are consumed in the steel. Subsequently, Ti atoms in FCC_A1#3 phase mainly combine with C atoms with decreasing temperature, as shown in Fig. 3c. FCC_A1#3 contains micro amounts of Nb elements, which is due to Ti(C, N) that precipitated earlier in the steel matrix, as a nucleation particle, promoted the precipitation of Nb(C, N). The

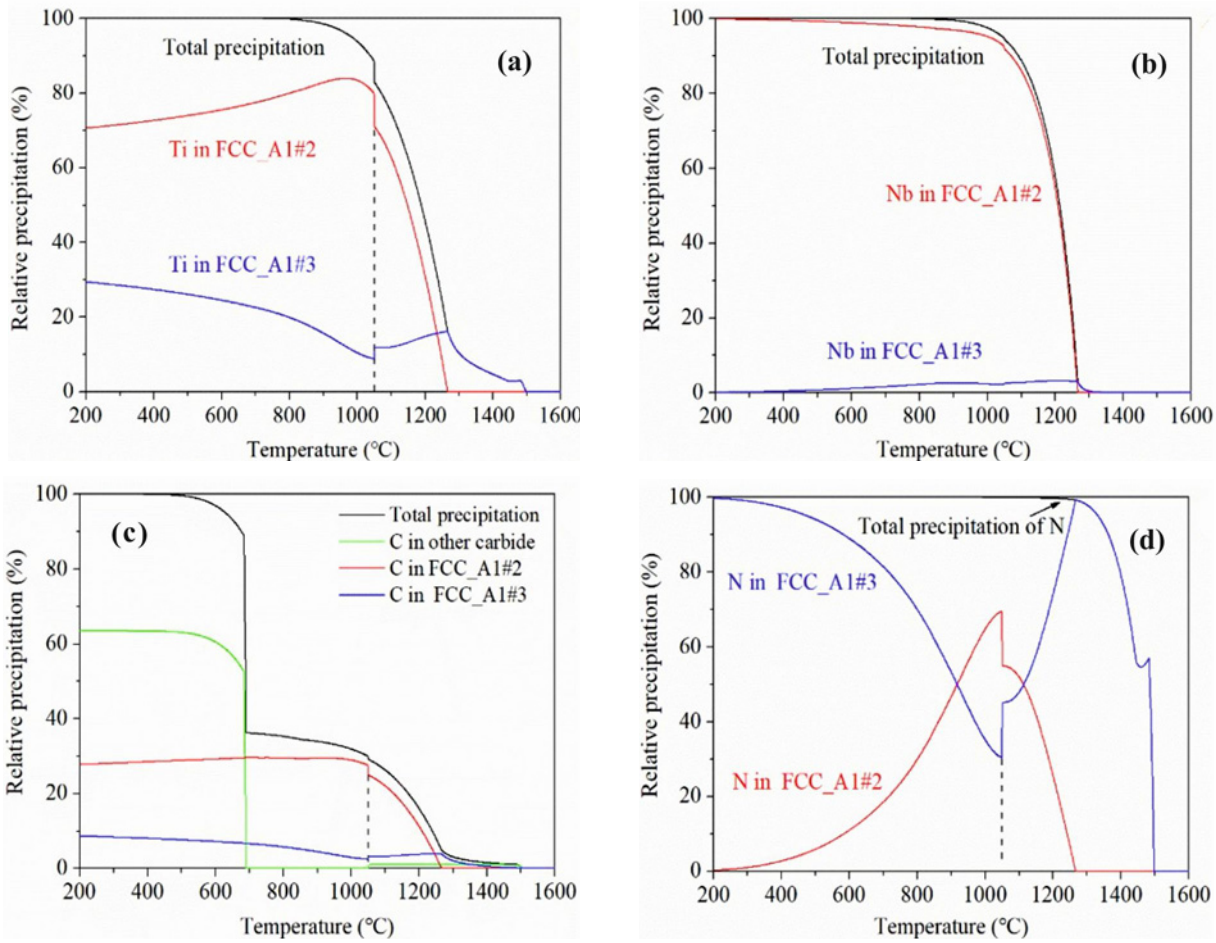

Fig. 4. Relative precipitation of elements in FCC_A1#2 and FCC_A1#3 phases in experimental steel: (a) Ti, (b) Nb, (c) C, and (d) N element.

content of FCC_A1#3 phase drops near 1450 °C, which might be due to the rapid transformation of high-temperature ferrite to austenite. The solubility product of FCC_A1#3 in the Fe matrix became larger, which caused the constituent elements to diffuse into the matrix. Furthermore, the fraction of FCC_A1#3 phase decreases at around 1266 °C, possibly because the FCC_A1#2 phase precipitates with FCC_A1#3 phase in the form of nucleation particles. A part of atoms from FCC_A1#3 diffused to FCC_A1#2 phase because of the isomorphic heteromorphic relation between FCC_A1#3 and FCC_A1#2.

FCC_A1#2 phase, similar to the constituent elements of FCC_A1#3, precipitates rapidly from 1266 °C and reaches a maximum amount near 950 °C. As seen in Fig. 3b, the content of C is much higher than that of N and remains at 18 %. In addition, the mole fraction of C is almost equal to the sum of the mole fraction of Ti and Nb in FCC_A1#2, which could be considered mainly composed of (Ti, Nb)C. The proportion of Nb element varies little with temperature by about 20 %, and Ti element proportion is maintained at around 60 %. It can be seen from Figs. 3c,d that FCC_A1#2 phase basically precipitates in the austenite region, while FCC_A1#3 phase precipitates slowly down to 200 °C.

The precipitation process of the second phase particles in the steel is a comprehensive reflection of the precipitation process of various elements. Figure 4 shows the redistribution process of the main elements, including Ti, Nb, C, and N in the experimental steel. Ti and Nb are almost completely precipitated at 800 °C, and their contents in the FCC_ A1#2 phase are much higher than that in the FCC_A1#3 phase in the low-temperature region. The C atoms mainly exist in austenite as a solid solution before the cementite begins to precipitate, and the rest of the C mostly precipitate in the FCC_A1#2 phase. The N atoms mainly exist in the FCC_A1#3 phase after complete precipitation. The precipitation containing Ti is earlier than the carbonitride of Nb according to the overall precipitation of various elements, which is consistent with the previous reports on other titanium and niobium steels [21, 22].

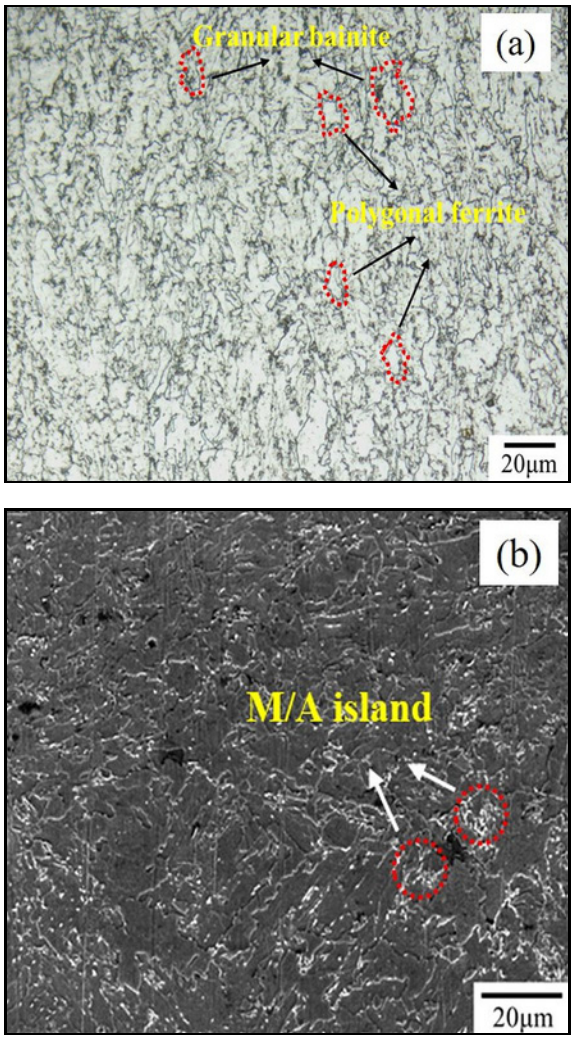

Fig. 5. Microstructure of hot rolled Nb-Ti composite microalloyed steel (×500): (a) metallography and (b) SEM image.

3.2. Microstructure evolution

Figure 5 shows the microstructure of the original experimental steel before heat treatment. Most of the matrix structure is occupied by polygonal ferrite (PF). In addition, there is a trace of granular bainite (GB) distributed along grain boundaries of PF. The carbon-enriched second phase disperses along the grain boundaries and within the bainitic matrix, usually called martensite/austenite (M/A) island. The SEM images of the morphology of the experimental steel tempered at different temperatures are shown in Fig. 6 to investigate the microstructure evolution during tempering. It is important to note that a few micron-scale PF and GB mainly dominate the microstructures along with dispersive carbide particles. However, there are slight differences among experimental steel under different tempering conditions. As can be seen from Fig. 6a, the granular bainitic matrix is manifested as an irregular lump. Many fine M/A island structures with low decomposition degrees were distributed in ferrite. The volume fraction of M/A islands in the experimental steel tempered at 500 ℃ is 19.4 % by statistically calculating using ImageJ, which is a public domain image processing software built up by the National Institute of Health. When the tempering temperature increased to 525 ℃, it was observable that the overall morphology of the microstructure did change significantly. Many M/A islands were decomposed as dispersed fine carbide in different shapes including spherical and short rods, as shown in Fig. 9d. It can be found from Fig. 6c that the fraction of PF distributed in the steel matrix increased obviously with the decreasing of GB. It was apparent that the size of GB of experimental steel tempered at 575 ℃ became larger, and there was still a small amount of undecomposed M/A islands. It can be roughly observed from Fig. 6e that the number of white granular precipitates increased significantly, which mainly precipitated at the boundary of ferrite. This is mainly because C was largely supersaturated and remained in the position of the original austenite phase, which would show a strong dissolution driving force during the tempering process. It can be seen from Fig. 6f that some precipitated particles were coarsened significantly with the increasing fraction and size of PF as the tempering temperature rose to 650 ℃. According to the transformation of the microstructure of the sample during tempering, the restorative effect of the tempering process got enhanced with the increasing temperature, and the dislocation located in

Table 3. Low-temperature impact energy and microhardness of experimental steels at different tempering temperatures

Tempering temperature (℃)	Hardness, HV5	Impact energy (J)
500	195	322
525	194	331
550	191	299
575	195	290
600	179	361
650	187	325

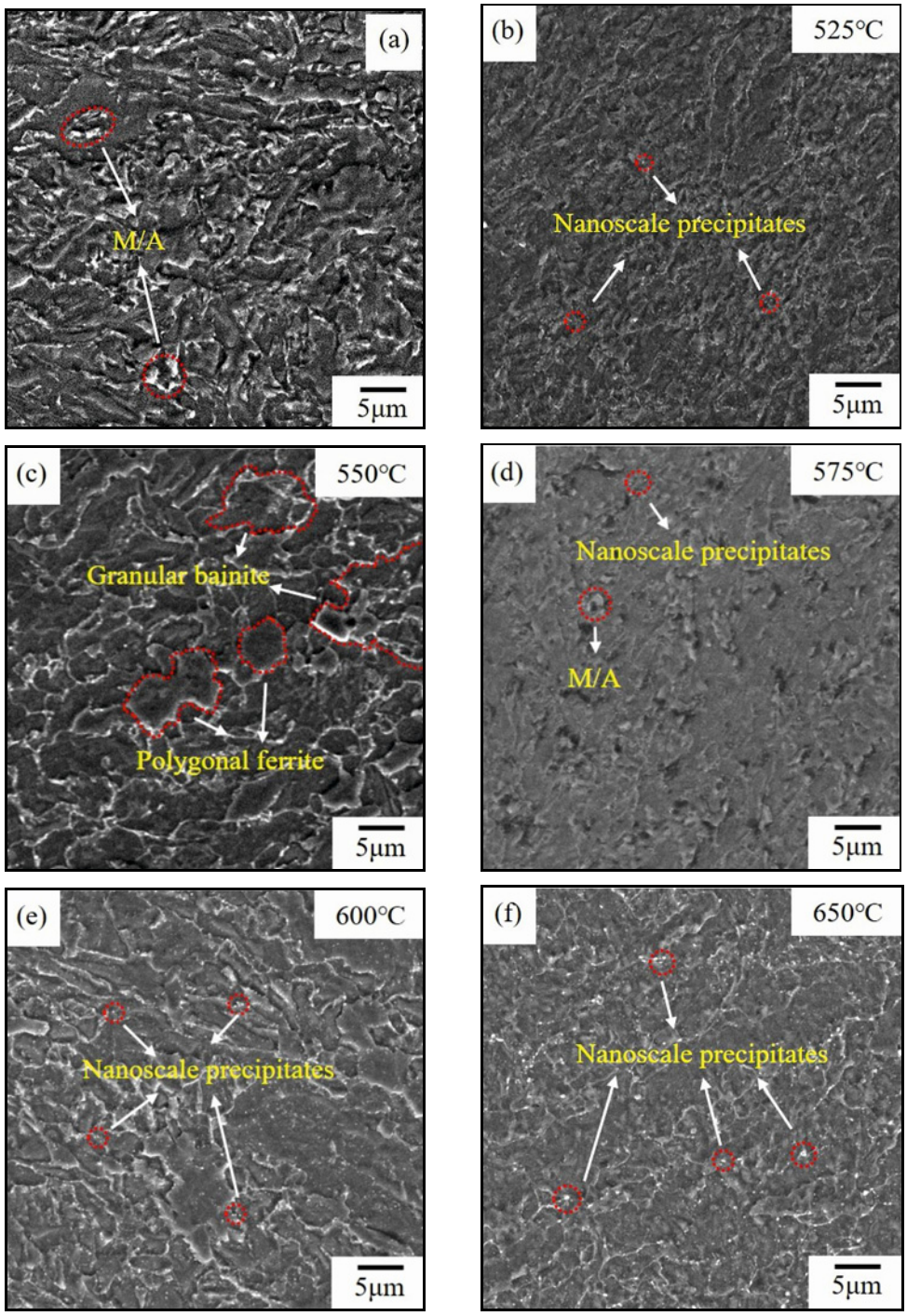

Fig. 6. SEM morphology of experimental steel at different tempering temperatures (×2000): (a) 500 °C, (b) 525 °C, (c) 550 °C, (d) 575 °C, (e) 600 °C, and (f) 650 °C.

the GB phase would move and recombine. Thus, the number of small-angle grain boundaries were reduced, and grains began to fuse and grow up to produce more PF.

3.3. Mechanical properties

Table 3 and Fig. 7 present the variation of low-temperature impact energy and microhardness of samples of the experimental steel at different tempering temperatures. It can be concluded from Fig. 7a that the low-temperature impact energy fluctuated and reached the maximum value of 361 J at 600 °C, which is much higher than the qualified standard of 47 J. According to the evolution of tempered microstructure, it was initially inferred that the grain

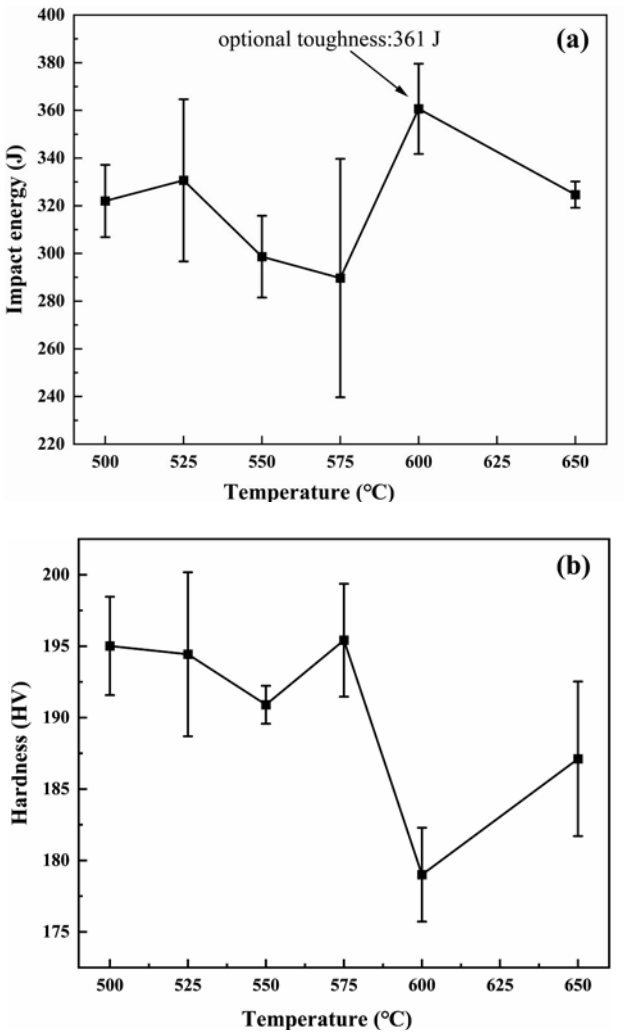

Fig. 7. Relationship between mechanical properties of experimental steels and tempering temperature: (a) low--temperature impact energy, and (b) Vickers hardness.

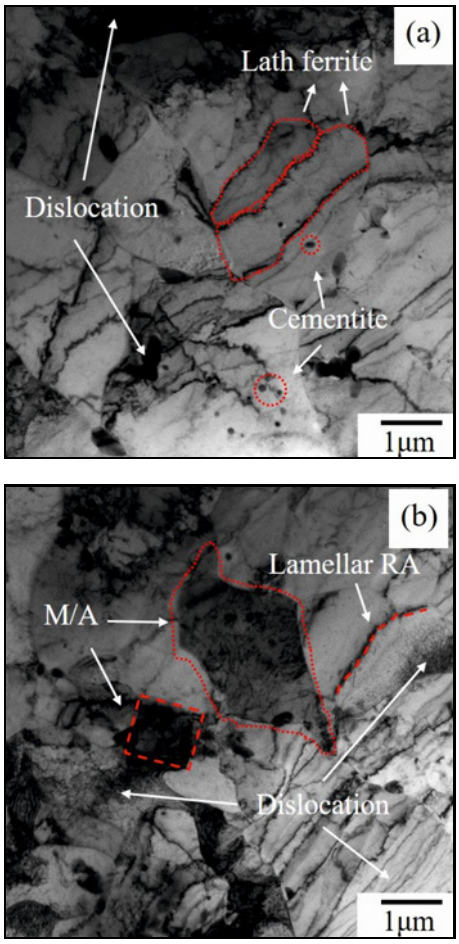

Fig. 8. TEM microstructure of the experimental steel tempered at 600 °C.

refining effect was slightly weakened due to the increasing size of the ferrite matrix. However, the precipitation strengthening effect was enhanced with the increasing number of nanoparticles, which led to fluctuations in their impact toughness. Subsequently, the low-temperature impact energy decreased at 650 °C, mainly caused by the coarsening and growing of the second phase particles. It can be seen from Fig. 7b that the microhardness dropped slightly. The hardness generally decreased with the increasing temperature caused by the softening of the matrix due to the decrease of dislocation density. However, the dispersed carbides formed during the tempering process resulted in secondary hardening. Thus, the decreasing trend of the hardness is not apparent. Therefore, the tempering temperature of the sample could be determined at 600 °C after being quenched from 900 °C.

3.4. TEM analysis of the second-phase particles

To further analyze the influence of the microstructure of the tempered samples on the optimal impact toughness, the fine structure of the microstructure of the sample was investigated by TEM, as shown in Fig. 8. It can be found that the fine structure of the tempered sample is different from the SEM morphology, in which the nearly parallel distributed lath bainite cannot be observed. There are intertangled network and cellular dislocations with high density in the ferrite matrix. Meanwhile, there is some continuous residual austenite (RA) with a width of about 10 nm distributed in the ferrite, which would be slowly decomposed into carbides during the tempering process. The cementite at the grain boundary would grow into spherical particles. Previous work has concluded that the spheroidal nano cementite carbide is beneficial for improving low-temperature toughness [23]. It was also reported [24] that the presence of a certain amount of stable RA in the steel matrix is beneficial to improve

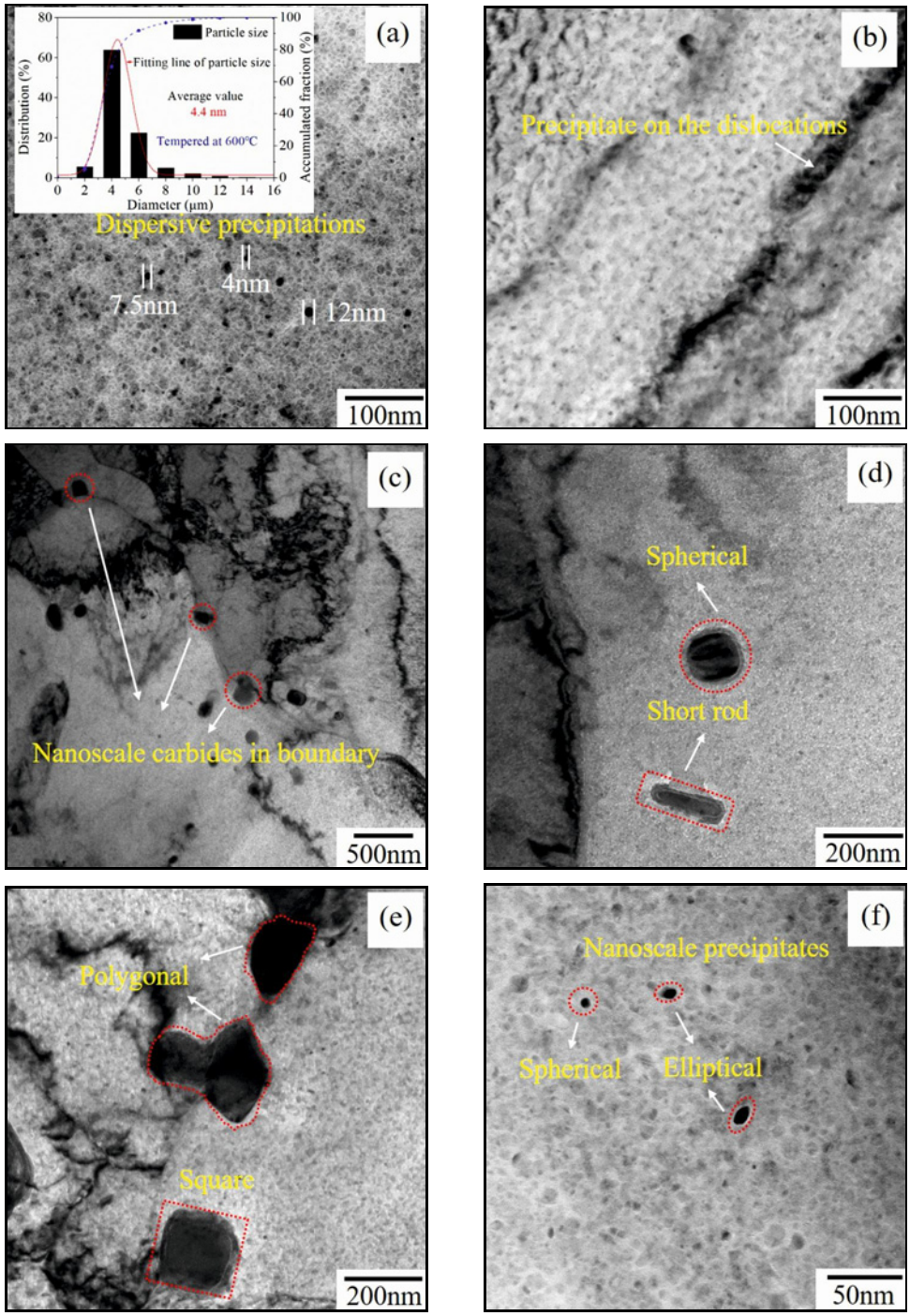

Fig. 9. Distribution and morphology of precipitated phase after tempering at 600 °C.

the impact toughness, which is due to the martensite in M/A islands induced by RA can absorb the impacting energy, thus improving the strength and toughness of the steel in the process of crack propagation.

The size, morphology, and distribution of typical nano precipitates in the tempered samples were examined by TEM, as shown in Fig. 9. Most fine precipitates were detected to be randomly distributed in the ferrite, as shown in Fig. 9a, which were manifested as spherical. Previous reports have demonstrated that nanoparticles with several nanometers contribute to precipitation strengthening, whereas the precipitates larger than 20 nm manifested relatively minor effects on improving the strength [25, 26]. The small particles in the samples were statistically analyzed, and their average diameter was stable at 4.4 nm, accounting for nearly 65 % of the total number of statistical particles. Furthermore, many nanoparticles formed

clusters and exhibited a chain-like distribution, which indicates that the precipitates are easy to nucleate and precipitate on the dislocations, as shown in Fig. 9b. It could be inferred that if the steel matrix is given a specific strain, it is conducive to the precipitation of the second phase particles, which conformed to the theory of strain-induced precipitation. It was observed from Fig. 9c that particles with the size of about 200 nm exist at the ferrite boundaries. The selected area diffraction (SAD) and EDS analysis verified that numerous precipitates located at the grain boundaries were M_3C-type cementite carbides, as shown in Fig. 10, which could be found that Fe, C, and Mn are the main composing elements. This is because the strong carbonitride elements such as Ti and Nb atoms exist in the form of displacement in the lattice of ferrite, which are not easy to move compared to the interstitial solid solution. However, the cementite would be firstly precipitated due to the strong diffusion ability of C atoms and consumed a large amount of C in the matrix, resulting in a small amount of precipitation of microalloyed carbide during tempering. The differences between cementite and microalloyed carbonitride observed by TEM were consistent with the results of the equilibrium precipitation of the second phase particles calculated by Thermo-Calc software. The precipitates aggregated on the grain boundaries inhibited the growth of austenite/ferrite by pinning the grain boundaries, and the microstructure is inherited in the ferrite grains, which contributes to the refining of the ferrite grain. Figures 9d–f show the morphologies of two kinds of typical precipitates. One is the spherical, short rod, and square precipitates with sizes ranging from 50–200 nm, and the other types are the spherical and elliptical particles with sizes smaller than 10 nm.

As mentioned above, the tempering temperature of the experimental steel was optimized at 600 ℃ after being quenched from 900 ℃, which showed the best low-temperature impact toughness. The fine bainitic ferrite with high-density dislocation formed during the tempering process could significantly improve the toughness while strengthening the microstructure of the matrix. In addition, many supersaturated carbides of appropriate size precipitated in the steel matrix and played a role in precipitation strengthening together with the undissolved carbonitrides in the microalloyed steel after tempering.

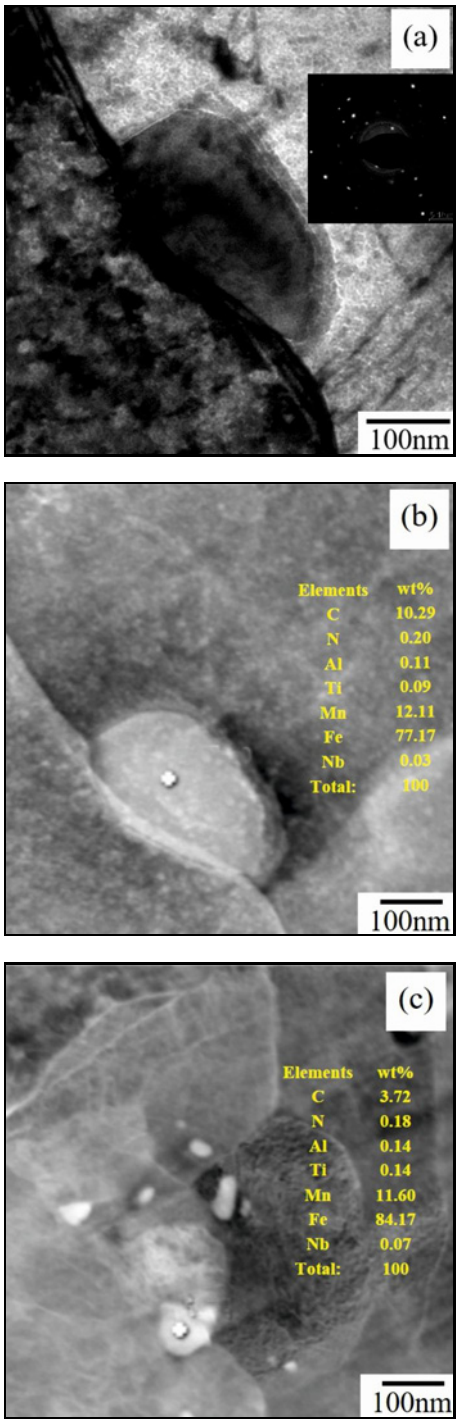

Fig. 10. Energy spectrum analysis of precipitated particles at the grain boundary of experimental steel after tempering at 600 ℃.

4. Conclusions

The precipitation behavior of the second phase particles in the high Ti microalloyed steel containing Nb was systematically investigated by thermodynamic calculation and experimentally. The effects of tempering temperatures on the microstructure and mechanical properties of the experimental steel were studied as well.

1. The phases of FCC_A1#3 and FCC_A1#2 were mainly composed of Ti, Nb, C, and N elements, which can be considered as Ti(C, N) and (Ti, Nb)C, considering the proportion of constituents in the phase.

2. Ti and Nb elements were almost completely precipitated at 800 ℃, and their contents in the FCC_A1#2 phase were much higher than in the FCC_A1#3 phase in the low-temperature region.

3. The microstructure of the Nb-Ti microalloyed steel consisted of polygonal ferrite (PF) and a few granular bainite (GB). The steel microstructure was mainly occupied by GB after tempering, on which M/A islands were distributed. The decomposition of M/A islands got enhanced, which transformed into a large number of nanoscale spherical cementite particles distributed at the grain boundary of the ferrite with the increasing tempering temperature, which is helpful to improve the toughness. Meanwhile, the size and fraction of PF also increased with the increasing temperature. Nevertheless, the variation of microhardness of the experimental steel was not evident with the temperature.

4. The experimental steel achieved the best low-temperature impact toughness of 361 J after quenching (900 ℃) and tempering at 600 ℃ for 60 min, which was due to the presence of a large number of bainitic ferrite with high-density dislocation and the second phase nanoparticles with an appropriate size and uniform distribution in the steel matrix.

Acknowledgements

The authors gratefully acknowledge the financial support from the Natural Science Foundation of Hebei Province, China (E2020318006) and the Venture & Innovation Support Program for Chongqing Overseas Returnees (cx2019026).

References

[1] Z. Shang, T. Li, S. Yang, J. Yan, H. Guo, Three-dimensional characterization of typical inclusions in steel by X-ray Micro-CT, Journal of Materials Research and Technology 9 (2020) 3686–3698. https://doi.org/10.1016/j.jmrt.2020.01.106

[2] J. Yan, T. Li, Z. Shang, H. Guo, Three-dimensional characterization of MnS inclusions in steel during rolling process, Mater. Charact. 158 (2019) 109944. https://doi.org/10.1016/j.matchar.2019.109944

[3] J. C. Villalobos, A. Del-Pozo, B. Campillo, J. Mayen, S. Serna, Microalloyed steels through history until 2018: Review of chemical composition, processing and hydrogen service, Metals 8 (2018) 351. https://doi.org/10.3390/met8050351

[4] J. Hu, K. Liu, L. Ma, R. D. K. Misra, W. Zhang, H. Du, W. Xu, Significant improvement in strength and toughness of nanoscale precipitate-strengthened steel by direct quenching and tempering process, Steel Res. Int. 92 (2021) 2000331. https://doi.org/10.1002/srin.202000331

[5] S. Ghosh, S. Mula, D. Kumar Mondal, Development of ultrahigh strength cast-grade microalloyed steel by simple innovative heat treatment techniques for industrial applications, Materials Science and Engineering A 700 (2017) 667–80. https://doi.org/10.1016/j.msea.2017.06.054

[6] Y. Funakawa, Interphase precipitation and application to practical steels, Mater. Trans. 60 (2019) 2086–2095. https://doi.org/10.2320/matertrans.M2018197

[7] Y. Han, J. Shi, L. Xu, W. Q. Cao, H. Dong, TiC precipitation induced effect on microstructure and mechanical properties in low carbon medium manganese steel, Materials Science and Engineering A 530 (2011) 643–651. https://doi.org/10.1016/j.msea.2011.10.037

[8] S. J. Spachinger, W. Ernst, N. Enzinger, Influence of Ti on the toughness of the FGHAZ and the CGHAZ of high-strength microalloyed S700MC steels, Weld World 61 (2017) 1117–1131. https://doi.org/10.1007/s40194-017-0480-7

[9] X. Gan, Q. Yuan, G. Zhao, H. Ma, W. Liang, Z. Xue, W. Qiao, G. Xu, Quantitative analysis of microstructures and strength of Nb-Ti microalloyed steel with different Ti additions, Metallurgical and Materials Transactions A 51 (2020) 2084–2096. https://doi.org/10.1007/s11661-020-05700-9

[10] W. L. Gao, Y. Leng, D. F. Fu, J. Teng, Effects of niobium and heat treatment on microstructure and mechanical properties of low carbon cast steels, Mater. Design 105 (2016) 114–123. https://doi.org/10.1016/j.matdes.2016.05.057

[11] A. Graux, S. Cazottes, D. De Castro, D. San Martín, C. Capdevila, J. M. Cabrera, S. Molas, S. Schreiber, D. Mirković, F. Danoix, M. Bugnet, D. Fabrègue, M. Perez, Precipitation and grain growth modelling in Ti-Nb microalloyed steels, Materialia 5 (2019) 100233. https://doi.org/10.1016/j.mtla.2019.100233

[12] M. Hua, C. I. Garcia, A. J. DeArdo, Precipitation behavior in ultra-low-carbon steels containing titanium and niobium, Metallurgical and Materials Transactions A 28 (1997) 1769–1780. https://doi.org/10.1007/s11661-997-0108-4

[13] Z. Hu, G. Xu, H. Yang, C. Zhang, R. Yu, The effects of cooling mode on precipitation and mechanical properties of a Ti-Nb microalloyed steel, J. Mater. Eng. Perform. 23 (2014) 4216–4222. https://doi.org/10.1007/s11665-014-1192-4

[14] M. Türkmen, M. A. Erden, H. Karabulut, S. Gündüz, The effects of heat treatment on the microstructure and mechanical properties of Nb-V microalloyed powder metallurgy steels, Acta Phys. Pol. A 135 (2019) 834–836. https://doi.org/10.12693/APhysPolA.135.834

[15] K. Bolanowski, Effect of heat treatment on mechanical properties and microstructure morphology of low-alloy high-strength steel, Arch. Metall Mater. 61 (2016) 475–480. https://doi.org/10.1515/amm-2016-0066

[16] J. Hu, L. Du, Y. Dong, Q. Meng, R. Misra, Effect of Ti variation on microstructure evolution and mechanical properties of low carbon medium Mn heavy plate steel, Mater. Charact. 152 (2019) 21–35. https://doi.org/10.1016/j.matchar.2019.04.004

[17] X. Qi, L. Du, J. Hu, R. D. K. Misra, Enhanced impact toughness of heat affected zone in gas shield arc weld joint of low-C medium-Mn high strength steel by post-weld heat treatment, Steel Res. Int. 89 (2018) 1700422. https://doi.org/10.1002/srin.201700422

[18] Y. Luo, J. Zhang, C. Xiao, Thermodynamic calculation and experimental investigation of second phase particles in low carbon Nb microalloyed steels, Steel Res. Int. 83 (2012) 238–243. https://doi.org/10.1002/srin.201100202

[19] Y. Wang, L. Zhuo, M. Chen, Z. Wang, Thermodynamic model for precipitation of carbonitrides in microalloyed steels and its application in Ti-V-C-N system, Rare Metals 35 (2016) 735–741. http://dx.doi.org/10.1007%2Fs12598-015-0495-4

[20] Y. Wang, L. Fu, M. Zhou, Z. Zhou, X. Pang, S. Zhong, A. A. Volinsky, Thermodynamics analysis of multiple microelements' coupling behavior in high fatigue resistance 50CrVA spring steel with nanoparticles, Materials 12 (2019) 2952. https://doi.org/10.3390/ma12182952

[21] J. H. Jang, Y. U. Heo, C. H. Lee, H. Bhadeshia, D. Suh, Interphase precipitation in Ti-Nb and Ti-Nb-Mo bearing steel, Mater. Sci. Tech. 29 (2013) 309–313. https://doi.org/10.1179/1743284712Y.0000000131

[22] Z. J. Xie, Y. P. Fang, G. Han, H. Guo, R. Misra, C. J. Shang, Structure-property relationship in a 960 MPa grade ultrahigh strength low carbon niobium-vanadium microalloyed steel: The significance of high frequency induction tempering, Materials Science and Engineering A 618 (2014) 112–117. https://doi.org/10.1016/j.msea.2014.08.072

[23] X. Deng, Z. Wang, R. Misra, J. Han, G. Wang, Precipitation behavior and mechanical properties of Ti-Mo medium-carbon steel during austenite to bainite transformation, J. Mater. Eng. Perform. 24 (2015) 1072–1078. https://doi.org/10.1007/s11665-014-1360-6

[24] Z. J. Xie, X. P. Ma, C. J. Shang, X. M. Wang, S. V. Subramanian, Nano-sized precipitation and properties of a low carbon niobium micro-alloyed bainitic steel, Materials Science and Engineering A 641 (2015) 37–44. https://doi.org/10.1016/j.msea.2015.05.101

[25] K. Zhang, Z. Li, X. Sun, Q. Yong, J. Yang, Y. Li, P. L. Zhao, Development of Ti-V-Mo complex microalloyed hot-rolled 900-MPa-grade high-strength steel, Acta Metallurgica Sinica (English Letters) 28 (2015) 641–648. https://doi.org/10.1007/s40195-015-0243-7